DISLOCATION VELOCITY AND SLIP ON THE $\{\bar{1}2\bar{1}2\}$ $\langle 1\bar{2}13\rangle$ SYSTEMS OF ZINC

Thesis by

Richard Clark Blish II

In Partial Fulfillment of the Requirements

For the Degree of

Doctor of Philosophy

California Institute of Technology

Pasadena, California

1967

(Submitted May 25, 1967)

ACKNOWLEDGEMENTS

The author wishes to thank Professor Thad Vreeland, Jr. for his generous and consistent help and friendship, without which this work would have been impossible. Appreciation is extended to: Professor D. S. Wood for his assistance and suggestions; Mr. G. R. May for his patience and skill applied to test specimen preparation; Mr. J. Held for help gathering the stress-strain curve data.

Special gratitude is extended to my wife, Sue, for her unfailing confidence and gradually acquired patience.

Thanks are also extended to the Atomic Energy Commision, which financially supported the experimental work.

ABSTRACT

Slip bands on the $\{\bar{1}2\bar{1}2\}$ $\langle 1\bar{2}13\rangle$ systems of zinc were produced by stress pulses and were observed by etch pitting. Edge and screw dislocation velocities as a function of stress and temperature (77° to 323°K) were deduced by measurement of the size of the slip bands. For the low temperature range of 77° to 110°K it is found that dislocation velocity is proportional to (stress) exp(-U/kT) where U = 0.182 ev. Screw dislocation velocity is found to be larger than edge dislocation velocity at a constant stress. It is suggested that a Peierls mechanism controls the dislocation velocity for the low temperature range. Above 110°K the slip bands start to become wider as cross glide takes precedence over the Peierls mechanism for the limitation of dislocation velocity. It is found that dislocation velocity decreases and the amount of cross glide increases with increasing temperature. It is suggested that the dislocations are retarded by an increasing number of dragging dipoles. The experimentally measured dislocation velocities are also related to the macroscopic measurements of the yield stress and the work hardening coefficient.

TABLE OF CONTENTS

TABLE OF CONTENTS--Continued

LIST OF FIGURES

LIST OF FIGURES--Continued

I. INTRODUCTION

There is extensive literature dealing with experiments which characterize the mechanical behavior of crystalline materials. The scope of the effort is very large because of the number of tests which must be performed on each material and the large number of material variables which influence the mechanical behavior. A better understanding of the processes which control the mechanical behavior of materials, with particular reference to plastic deformation, could greatly enhance our ability to predict material properties. The ability to predict the material properties would allow us to choose the optimum material for a given purpose.

The nature of plastic deformation is usually studied in experiments in which only macroscopic measurements of stress and strain are utilized. However, this type of experiment is very difficult to interpret. Plastic deformation is a complex process, so the interpretation of macroscopic measurements is handicapped by a lack of knowledge about the important and interdependent microscopic variables. Interpretation of these experiments always depends upon the assumption of certain microscopic models, whose validity cannot necessarily be deduced from the macroscopic experiments themselves. A more reliable approach to the problem involves independent microscopic measurements to establish the validity of the models. This microscopic information can then be used to refine the model which permits interpretation of the macroscopic behavior.

Models based on the dynamics of crystal dislocations have

successfully explained some aspects of plastic deformation. Macroscopic experiments alone were not able to account for the observed properties. Johnston and Gilman (1)* illustrated the importance of dislocation dynamics in the stress-strain behavior at very low strains in lithium fluoride crystals. Li (2) used dislocation dynamics to explain macroscopic observations during transient creep and Taylor (3) also used dislocation dynamics to explain observations regarding plastic wave propagation.

Work hardening, the property that increased stress is required to cause further plastic deformation during a stress-strain test, has been studied by many investigators using both macroscopic and microscopic measurements. This process is very complicated because many effects are superimposed. Large numbers of dislocations are produced during straining and the dislocations interact in many ways with each other or with other lattice defects. The nature of these interactions depends upon the active slip systems, temperature, distribution of impurities and other defects, and the rate of change of many of these parameters. Nabarro, et al. (4) have discussed many aspects of work hardening and other elements of crystal plasticity in an extensive review article.

Johnston and Gilman (1) predicted stress-strain relations at

*Numbers appearing in parentheses indicate references listed at the end of the thesis.

very low strains on the basis of the effects of testing machine characteristics and dislocation velocity and multiplication. The dislocation dynamics were obtained from separate experiments. The calculated stress-strain relations matched the experimental results very well, although discrepancies were noted at larger strains and were attributed to work hardening. However, a prediction of stress-strain relations at higher strains, where dislocation interactions become dominant, must be based on a theory of work hardening. The stress-strain relations are the most important data to consider in a theory of work hardening according to Seeger (5). However, Kocks (6) points out the importance and difficulty of incorporating the effects of dislocation dynamics into such a theory.

Nabarro, et al. (4) state that work hardening for stage II in FCC metals shows very little temperature dependence of work hardening. Stage II for FCC metals may be similar to pyramidal slip in zinc (intersecting slip systems) but Stofel and Wood (7) found that slip on second order pyramidal planes $\{\bar{1}2\bar{1}2\}$ $\langle 12\bar{1}3\rangle$ of zinc exhibits a strong temperature dependence, namely a decrease in yield stress and work hardening with a decrease in temperature below room temperature. Gilman (8) also observed this effect but erroneously attributed the plastic deformation to kinking rather than second order pyramidal slip. Slip on these planes has also been observed by Bell and Cahn (9) and Price (10). Zinc may also slip on prism planes at temperatures greater than 250°C (11), however the second order pyramidal slip systems are the dominant non-basal slip systems below this temperature.

Second order pyramidal slip (or any other forms of non-basal slip) can only be initiated when basal slip is suppressed, since a much greater critical resolved shear stress is required for pyramidal slip than for basal slip. The extreme plastic anisotrophy of zinc is related to the hexagonal close packed crystal structure with a large c/a ratio. The different symmetry and spacing of the planes would be expected to affect the relative dislocation mobility by virtue of changes in the Peierls-Nabarro stress, the stacking fault energies, and the possible dislocation dissociations, reactions and interactions. The symmetry of the crystal also affects the rate of work hardening for the two different kinds of slip. No other plane of easy slip intersects the basal plane, so basal slip can take place without interference from slip on intersecting planes. On the other hand, there are six intersecting second order pyramidal slip planes. The number of active pyramidal slip systems depends upon the particular orientation of the test crystal and stress state and is always two or more when the basal slip system is not stressed.

This investigation is concerned with pyramidal slip in hexagonal close-packed crystals. In particular, we have sought a correlation between the anomalous work hardening and the pertinent dislocation dynamics for second order pyramidal slip in zinc. The crystals were subjected to load pulses and were oriented with respect to the loading direction such that basal slip was minimized. The rate of formation and the nature of pyramidal slip bands has been measured as a function of stress and temperature in single crystals of high

purity zinc. The active pyramidal slip systems were oriented with respect to the loading direction such that motion of pure edge and pure screw dislocations could be studied. The dislocations were revealed by chemical etch pitting of the surfaces (12,13) and Berg-Barrett x-ray diffraction topography (14). Stress-strain relations were also obtained and the observed yield stresses and work hardening coefficients are qualitatively related to the dislocation dynamics.

II. TEST SPECIMEN PREPARATION

The compression test specimens were 99.999% pure zinc single crystals containing an initial dislocation density of approximately $10^4 cm^{-2}$. The orientation of the test specimen is illustrated in Figure 1. The hexagonal axis of zinc ($\bar{c}$) is normal to the basal plane and $\bar{a}$ is one of the directions of close packing in the basal plane.

The single crystals were grown in graphite-coated pyrex molds 3.5 cm in diameter and 30 cm long. The large parent single crystal was acid sawed into roughly shaped test specimens and the individual test specimens were cleaved in liquid nitrogen to determine the precise crystallographic orientation. The test specimen was then acid lapped to the desired shape, shown in Figure 1, using orientation control techniques described by Adams (15). The acid lapping machine employed a pair of parallel flexures (to maintain proper orientation) and a rotating cloth-covered wheel which supplied the acid (4N HNO_3). An orientation reference block (15), to which the specimen was glued, was attached to the flexures and the specimen was allowed to touch the rotating wheel very lightly. The specimen was also rotated about an axis parallel to the axis of the rotating wheel. The concentration of the acid, pressure of the crystal aganist the cloth, and the rotation speeds were chosen to obtain flat surfaces without damaging the very fragile crystals.

For some of the tests a slightly different specimen shape was produced, that of rectangular parallelepiped. The orientation of

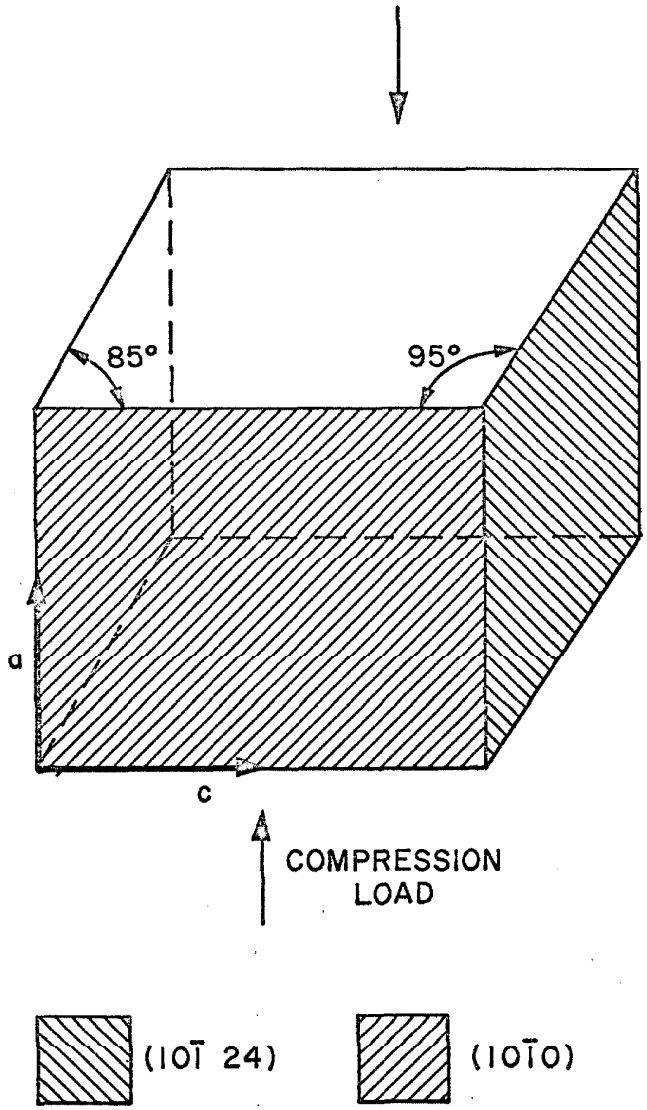

Figure 1 Test specimen orientation, $\bar{c}$ is the hexagonal axis of zinc, $\bar{a}$ is the direction of close-packing in the basal plane

free surfaces of these crystals were two each of $\{10\bar{1}0\}$, $\{1\bar{2}10\}$, and $\{0001\}$.

All the test specimens were annealed at 370°C in purified hydrogen for periods of 4 to 24 hours after all the acid-lapping operations. The hydrogen was purified by diffusion through a hot thin-walled palladium tube in a commercially available unit.

III EXPERIMENTAL TECHNIQUES

Pulse Tests

Square compression load pulses of controlled amplitude and duration produced by a rapid loading machine (16) were applied to the crystals at various temperatures. Temperature of the crystal was established by immersion in liquids such as nitrogen, methanol, or water. The crystal was in a sealed black body cavity filled with air for the tests at 88°, 100°, and 110°K. Copper-constantan thermocouples were used to measure the temperature accurate to ± 2°K, however the measurements were less accurate for the tests at 88°, 100°, and 110°K (±4°K).

Replication fluid manufactured by Ladd Industries was applied to the crystal before the test to prevent contamination of the observation surfaces. A soft pad was placed at each end of the compression test specimen to distribute the load uniformly over the entire loading surface. Load vs time was recorded during the test on an oscillograph, each to an accuracy of ±1%. After the load pulse was applied, Berg-Barrett x-ray diffraction micrographs (see Appendix A) and chemical etch pitting (12,13) of the lateral surfaces were employed to reveal the dislocations and the slip bands. Plastic replicas of the etched surfaces were made to provide a permanent record for subsequent examination and measurement.

The crystals were re-tested after cleaning and annealing. Following any given test the crystal was placed in a vacuum chamber (3×10^{-6} torr) and heated to 60°C for 12 hours to remove most of

the mercury which was present on the surface from the etching solution. The vacuum treatment was followed by annealing at 370°C in flowing hydrogen to complete the distillation of the mercury and reduce the dislocation density to that of the virgin crystal. The vacuum and annealing treatment left the surfaces sufficiently flat and clean for subsequent dislocation observation.

Slip band lengths, recorded on the plastic replicas of the etched surfaces, were measured accurate to ±3% by using a translating stage on a microscope. Hence, the average velocity of the dislocations, which is equal to slip band length divided by duration of the stress pulse, was measured accurate to ±4%. Specimen cross-sectional area was measured accurate to ±2% and the average stresses reported are accurate to ±3%.

Stress-Strain Relations

Stress-strain relations at various temperatures were obtained from slow-loading compression tests performed in an Instron testing machine using a crosshead speed of 0.0075 cm/min. Strain was detected by strain gages bonded to the crystal, and was recorded as a function of load. Soft pads at the ends of the crystal were also utilized for these tests. Temperatures were obtained by immersing the crystal in liquid baths such as oil heated to 50°C, ice water, dry ice-methanol, solid and liquid Freon 12 in equilibrium, liquid nitrogen, or liquid argon.

IV EXPERIMENTAL RESULTS

Nature of the Deformation

Deformation of crystals compressed in the $\bar{a}$ direction and in the $\bar{c}$ direction was accomodated by the formation of slip bands. Compression in the $\bar{c}$ direction also caused the formation of twins as well as slip bands. The primary objective of this investigation was a study of slip; observations regarding twinning are discussed in Appendix B. Nearly all of the tests involved $\bar{a}$ axis compression, for which twinning of zinc is impossible, as the formation of twins requires an extension in the $\bar{a}$ direction or a compression in the $\bar{c}$ direction.

The slip bands intersect the etched observation surfaces $\{10\bar{1}0\}$ at angles of $\pm 61.8^{\circ}$ from $\bar{a}$ (see Figures 3,4,5). The trace of the slip bands on the etched observation surfaces $\{10\bar{1}\,24\}$ is perpendicular to $\bar{a}$ (see Figure 6). These traces indicate that the slip bands belong to the second order pyramidal systems $\{\bar{1}2\bar{1}2\}\ \langle 12\bar{1}3\rangle$.

Two of the six $\{\bar{1}2\bar{1}2\}\ \langle 12\bar{1}3\rangle$ slip systems receive the maximum resolved shear stress for tension or compression in the $\bar{a}$ direction. The other four systems receive only 1/4 as much resolved shear stress and are inactive relative to the two highly stressed systems. Figure 2 shows the zinc hexagonal unit cell, the loading direction, the two active slip systems, and two of the specimen surfaces on which dislocations are observed by etch pitting (12,13). AC is the Burgers vector for the $(\bar{1}2\bar{1}2)$ slip plane, so a dislocation line parallel to AC is a pure screw dislocation. AB is perpendicular

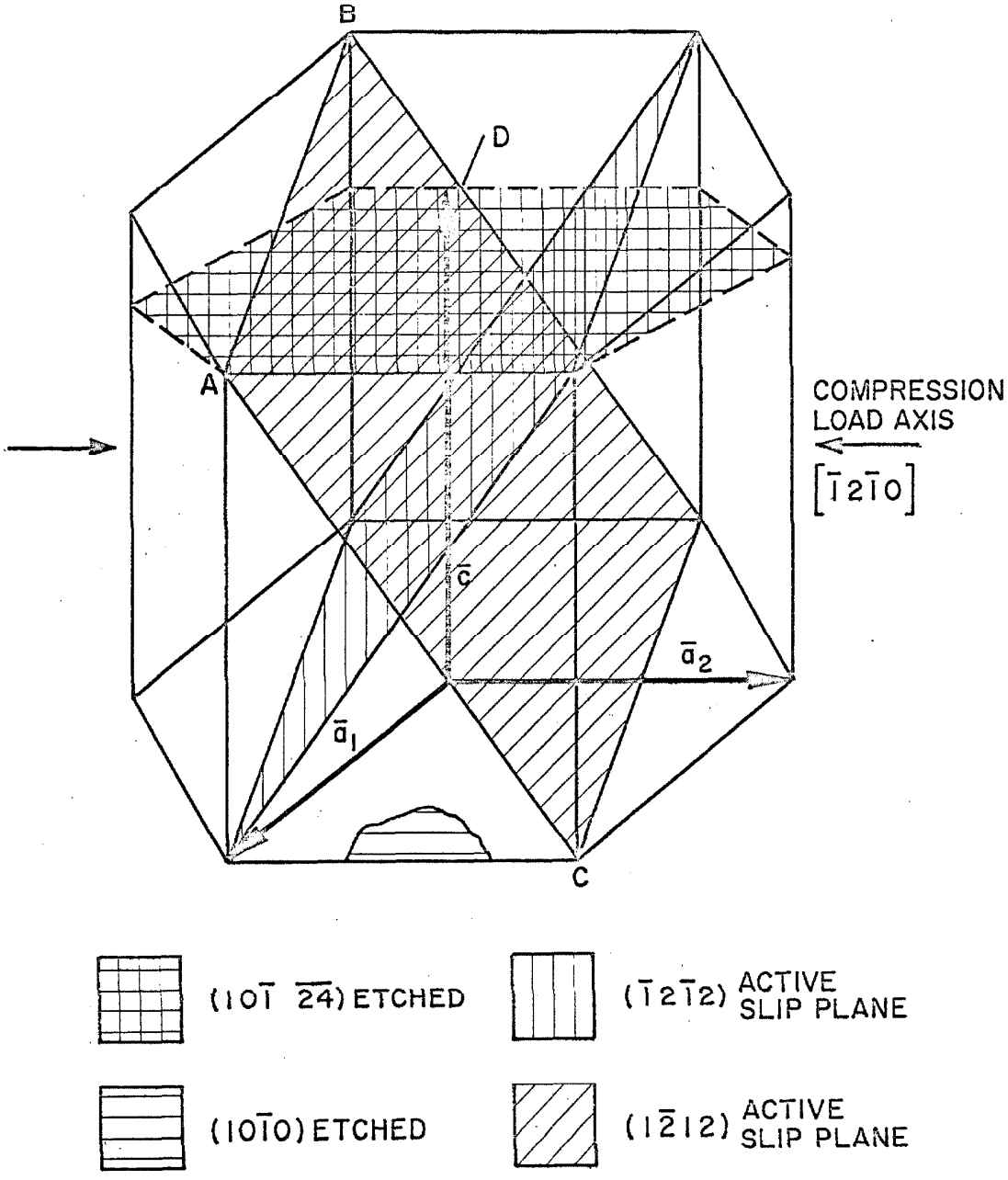

Figure 2 Unit cell of zinc showing the etched surfaces and the active slip planes for the given stress state

to the Burgers vector so a dislocation line parallel to AB is a pure edge dislocation. It should be noted that edge dislocations lie in the basal plane while the screw dislocations do not.

The extent of a slip band cutting $(10\bar{1}0)$ along AC is limited by the motion of dislocation lines which are parallel to AB, that is, pure edge dislocations. Similarly, the extent of a slip band cutting $(10\bar{1}\,\bar{2}4)$ along AD is limited by the motion of dislocations parallel to AC, that is, pure screw dislocations. Hence, it is assumed that the extent of slip bands intersecting $\{10\bar{1}0\}$ and $\{10\bar{1}\,24\}$ is related to the motion of pure edge and pure screw dislocations, respectively.

The geometrical shape of the slip bands was found to be a sensitive function of temperature, and only slightly dependent upon the stress level or the duration of the stress. At temperatures of 200°K and less the slip bands have little, if any, perceptible width. They become progressively wider as the temperature is increased above 200°K. Figures 3, 4, and 5 illustrate slip bands formed at 200°, 273°, and 323°K, as observed by etching the $(10\bar{1}0)$ surface.

Low-angle boundaries are usually the sources for slip bands which are formed at low temperatures. Figure 3 shows slip bands initiated at the low angle boundary which runs across the center of the picture. The source of the slip band is recognized by the characteristically greater width and higher dislocation density than that of the leading end of the band. Figure 3 also indicates that slip bands interfere with each other to varying degrees. At

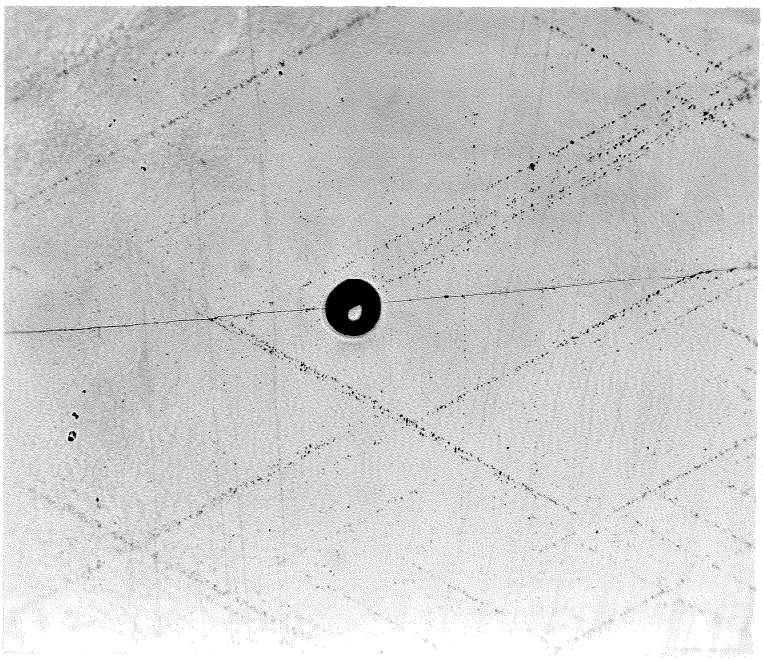

Figure 3 $(10\bar{1}0)$ surface, $\bar{a}$ vertical, slip bands in specimen 29-26 formed at 200°K, 22.4 Mdyne/cm^2, 0.610 sec , 50X

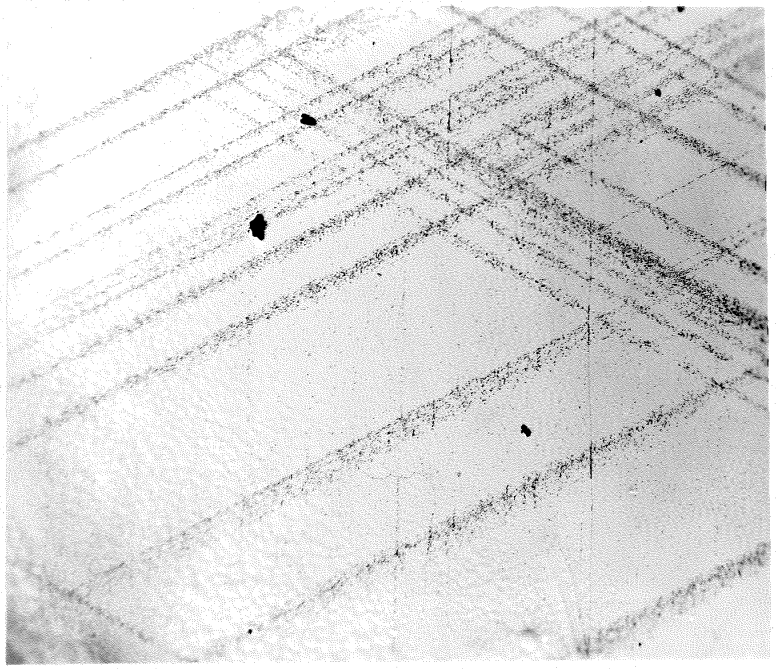

Figure 4 ($10\bar{1}0$) surface, $\bar{a}$ vertical, slip bands in specimen 36-1 formed at 273°K, 16.8 Mdyne/cm^2, 1.56 sec , 50X

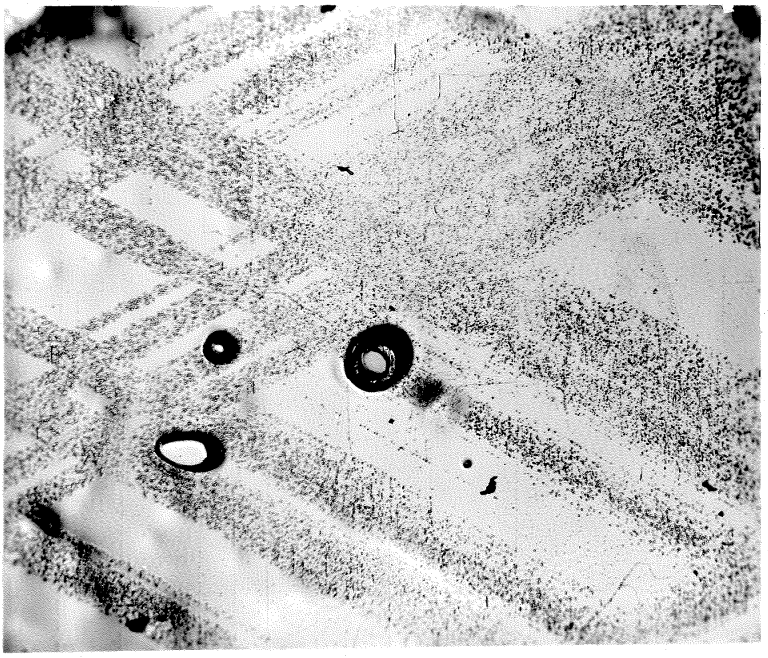

Figure 5 $(10\bar{1}0)$ surface, $\bar{a}$ vertical, slip bands in specimen 36-3 formed at 323°K, 35.8 Mdyne/cm^2, 0.109 sec , 50X

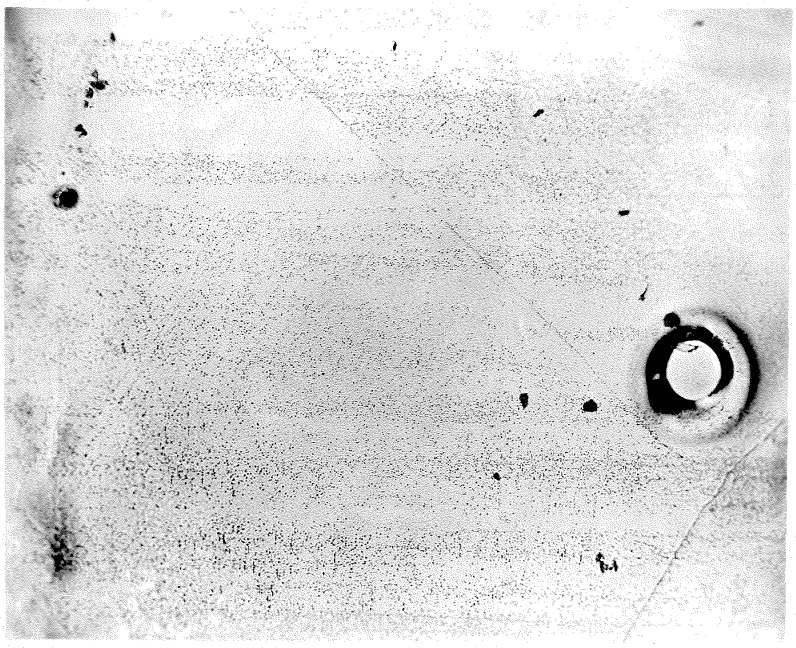

Figure 6 $(10\bar{1}\,24)$ surface, $\bar{a}$ vertical, slip bands in specimen 29-26 formed at 323°K, 24.2 Mdyne/cm^2, 300 sec , 50X

higher temperatures, sources within the subgrain are activated and the slip bands are usually symmetrical about the center (Figures 4 and 5). Here the greater width and higher dislocation density is observed at the center of the band.

Dislocation Velocity

The velocity of edge and screw dislocations was derived by measuring the length of the slip bands on the $\{10\bar{1}0\}$ and $\{10\bar{1}\,24\}$ surfaces, respectively. Slip band length is divided by the pulse duration to obtain average dislocation velocity. The length of the slip band is defined as the distance from the source of the slip band to its end(s). The longest slip bands were measured, as these are assumed to have nucleated at the observation surface rather than beneath it. Dislocation velocity for a particular test was calculated from the average length of at least 10 of the longest slip bands observed on each pair of equivalent crystallographic surfaces. There is a slight amount of stress concentration which is effective up to 1 mm from each end as deduced by the distribution of the slip bands. Hence, slip bands were only considered if they were at least 2 mm from the ends. (Typical specimen length is 10 to 15 mm.)

Edge and screw dislocation velocities as a function of resolved shear stress and temperature are presented in Table I. All measurements were obtained from slip bands produced in crystals oriented for $\bar{a}$ axis compression except for those cases which will now be

TABLE I

DISLOCATION VELOCITY AS A FUNCTION OF STRESS AND TEMPERATURE

Crystal Number and Test	Temp. °K	Resolved Shear Stress Mdyne/cm^2	Load Duration sec	Edge Dislocation Velocity cm/sec	Screw Dislocation Velocity cm/sec
36-1T6	77	16.3	18000	____	2.2×10^{-6}
36-4T6	77	20.7	35400	1.1×10^{-6}	6.3×10^{-6}
36-1T6	77	65.5	18000	2.7×10^{-6}	1.3×10^{-5}
29-9T7	88	13.8	700	7.1×10^{-5}	3.3×10^{-4}
29-9T6	88	30.9	1000	8.8×10^{-5}	4.6×10^{-4}
35-0T2	100	24.0	31.0	4.8×10^{-3}	1.3×10^{-2}
35-6T6	100	37.7	3.24	5.7×10^{-3}	9.6×10^{-3}
36-4T5	110	12.5	10.0	1.3×10^{-2}	4.0×10^{-2}
36-4T1	110	17.1	8.20	1.8×10^{-2}	5.8×10^{-2}
29-8T6	110	29.0	8.30	1.3×10^{-2}	5.1×10^{-2}
29-6T5	110	31.9	2.61	____	2.1×10^{-1}
29-26T7	110	37.9	5.00	3.8×10^{-2}	1.2×10^{-1}
29-9T10	175	14.7	2.13	8.4×10^{-2}	2.8×10^{-1}
36-4T4	175	30.4	1.03	2.5×10^{-1}	____
29-9T5	200	8.6	7.4	1.3×10^{-2}	6.3×10^{-2}
29-8T4	200	10.7	8.0	3.3×10^{-2}	5.1×10^{-2}
35-0T3	200	16.7	1.04	8.8×10^{-2}	4.6×10^{-2}
29-26T2	200	22.4	0.610	3.3×10^{-1}	7.4×10^{-1}
35-6T3	200	31.0	0.346	5.1×10^{-1}	1.4×10^{0}

TABLE I (continued)

Crystal Number and Test	Temp. °K	Resolved Shear Stress Mdyne/cm^2	Load Duration sec	Edge Dislocation Velocity cm/sec	Screw Dislocation Velocity cm/sec
35-6T6	230	11.7	3.24	6.1×10^{-2}	6.1×10^{-2}
29-8T9	230	24.8	1.17	1.8×10^{-1}	3.5×10^{-1}
29-9T9	273	9.0	41.3	4.3×10^{-3}	5.8×10^{-3}
36-3T3	273	11.8	5.20	5.8×10^{-2}	6.7×10^{-2}
36-1T3	273	16.8	1.56	3.0×10^{-1}	3.3×10^{-1}
36-4T3	273	23.3	0.017	6.8×10^{0}	$1.5 \times 10^{+1}$
29-9T2	294	7.85	400	2.5×10^{-4}	____
29-8T11āt	294	10.3	100	2.0×10^{-3}	1.5×10^{-3}
29-1T2	294	11.4	25.1	6.1×10^{-3}	____
35-6T8āt	294	12.4	25.0	5.6×10^{-3}	7.1×10^{-3}
29-1T1	294	13.6	26.0	1.0×10^{-2}	____
29-9T1	294	16.3	3.01	4.1×10^{-2}	____
35-6T1	294	22.4	0.215	5.6×10^{-1}	____
29-19T1c̄c	294	24.1	0.145	3.8×10^{-1}	____
29-20T1c̄c	294	29.0	0.145	1.0×10^{0}	____
29-8T1	294	29.3	0.017	8.1×10^{0}	5.8×10^{0}
29-20T2c̄c	294	31.0	0.018	7.6×10^{0}	____
29-26T6	323	24.2	300	5.1×10^{-4}	7.1×10^{-4}
36-1T4	323	27.5	20.6	2.8×10^{-2}	2.8×10^{-2}
35-6T7	323	31.6	15.6	1.9×10^{-2}	1.9×10^{-2}
36-3T4	323	35.8	0.109	3.0×10^{0}	3.0×10^{0}

discussed. Two test crystals were oriented for $\bar{a}$ axis tension and are denoted by $\bar{a}$t following the crystal number and test. Three tests were performed under the condition of $\bar{c}$ axis compression and are denoted by $\bar{c}$c. In one case, crystal 36-1 test number 6 (36-1T6), $\bar{a}$ axis compression produced slip bands on the "inactive" slip systems as well as the active ones. For this particular case screw dislocation velocity was obtained for two different resolved shear stresses during the same test.

Figures 7, 8, and 9 show graphical representations of dislocation velocity as a function of stress for the various temperatures employed. A rather large scatter from one test to another is found in the measured dislocation velocities. The variation in slip band lengths for any one test is smaller ($\pm 15\%$) than that from test to test ($\pm 30\%$). The source of this scatter is discussed in the next section.

Stress-Strain Relations

The test conditions appropriate to the stress-strain tests were described in an earlier section. The stress-strain curves can be closely approximated by the linear segments shown in Figure 10. Two tests at 77°K were attempted, and no plastic strain could be detected even at stresses as high as 350 Mdyne/cm^2, so the curves for 77°K represent elastic behavior. The stress required to produce a plastic strain of 0.01% is plotted as a function of absolute temperature in Figure 11. The slope of the stress-plastic strain curve, the work hardening coefficient, is plotted against absolute temperature in Figure 12.

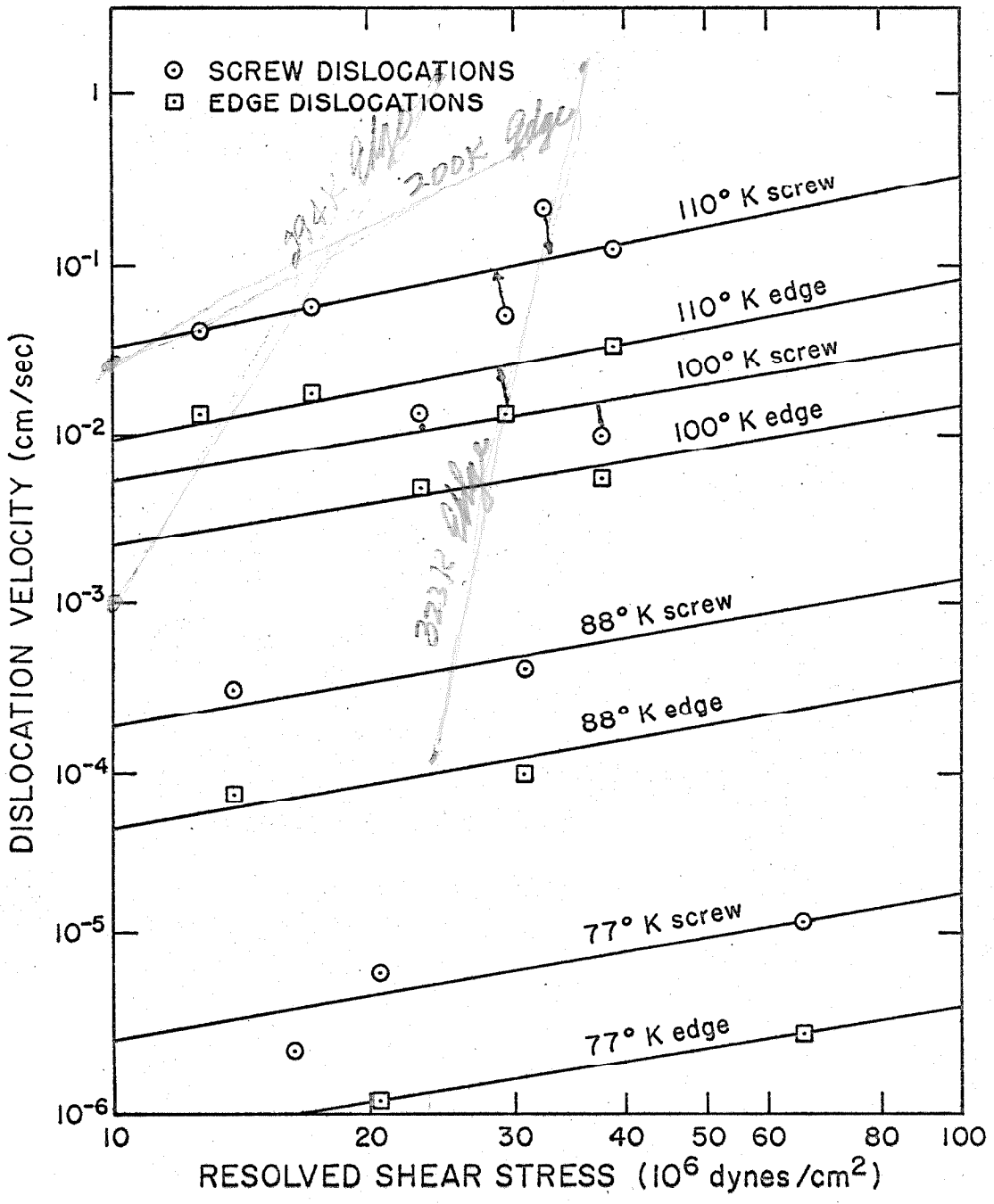

Figure 7 Dislocation velocity as a function of resolved shear stress for various temperatures and orientations

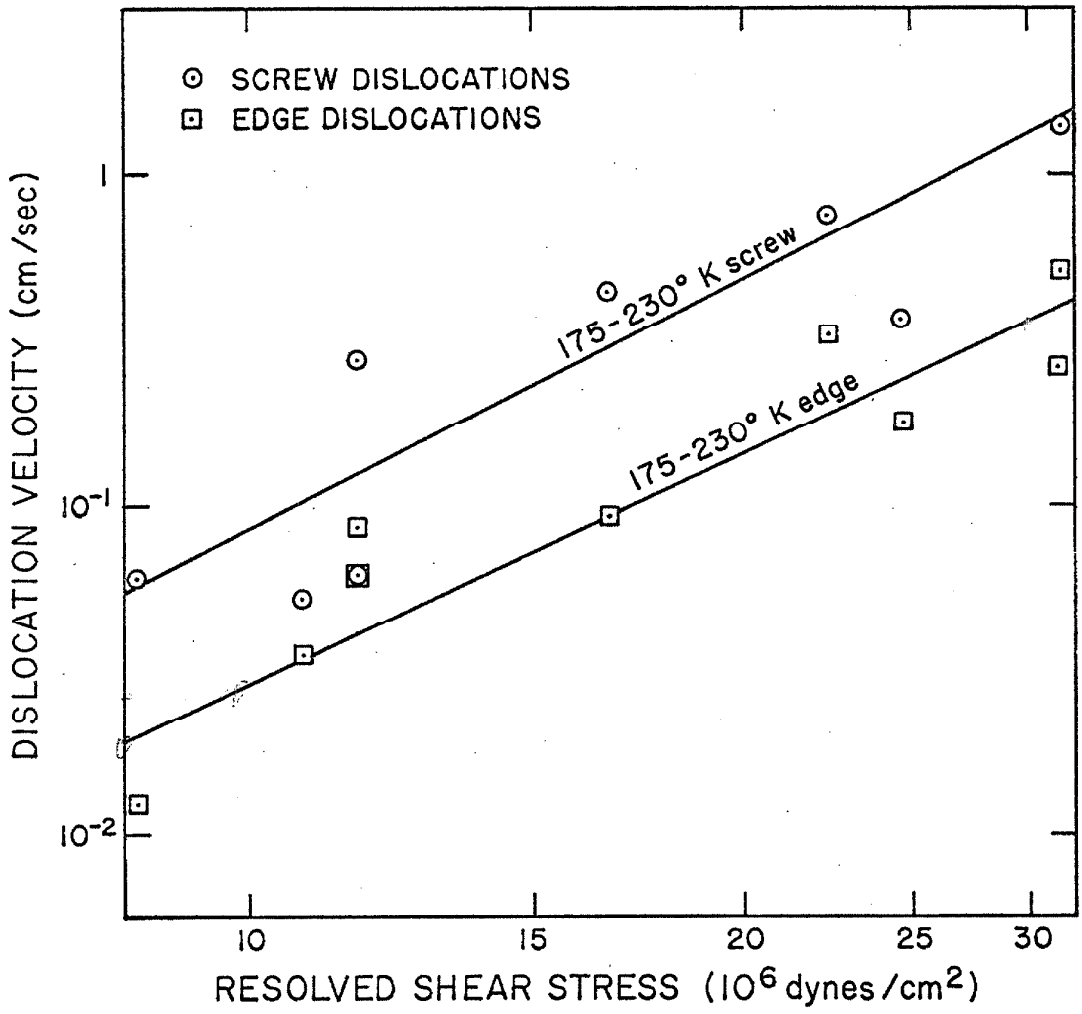

Figure 8 Dislocation velocity as a function of resolved shear stress for various temperatures and orientations

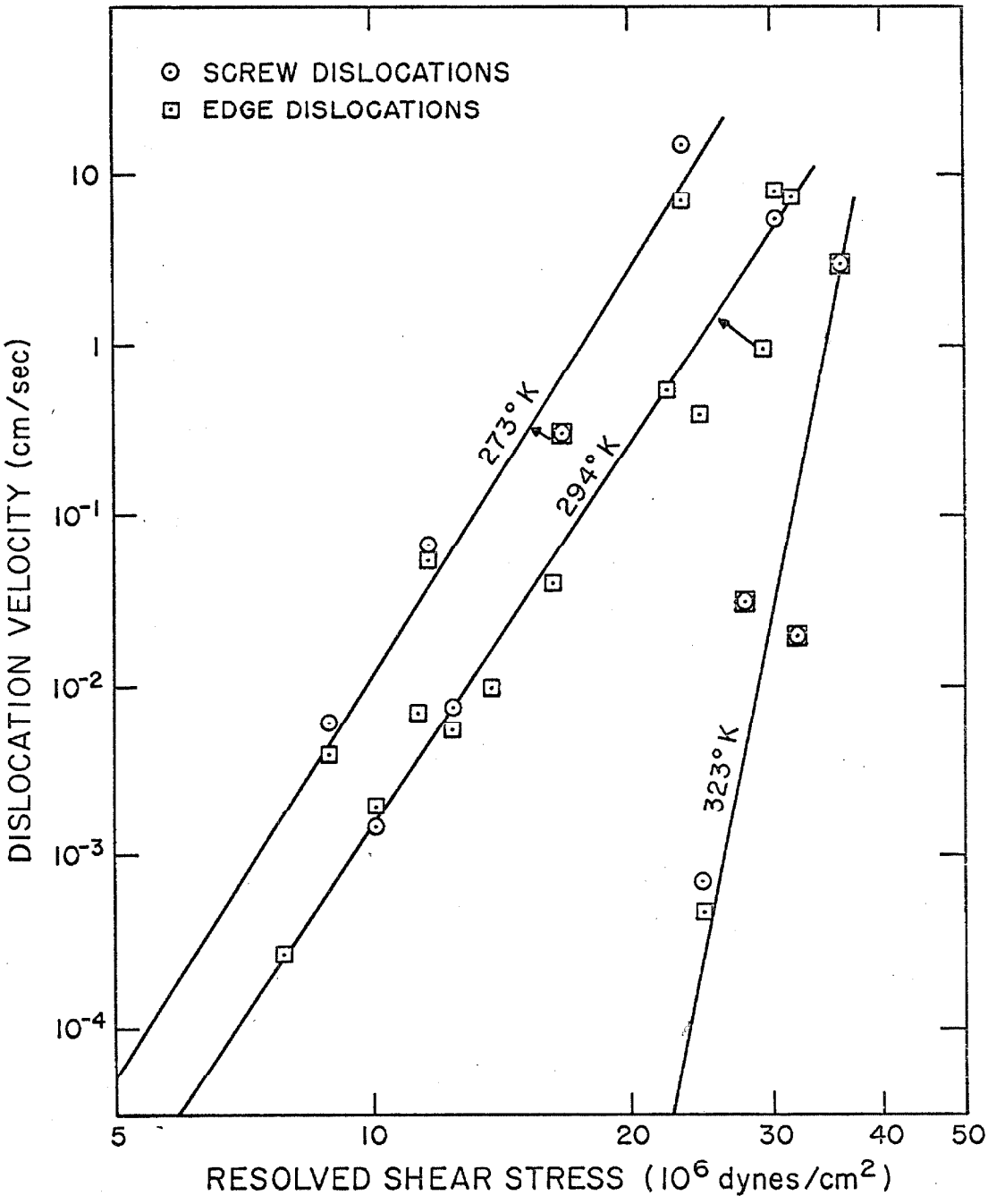

Figure 9 Dislocation velocity as a function of resolved shear stress for various temperatures and orientations

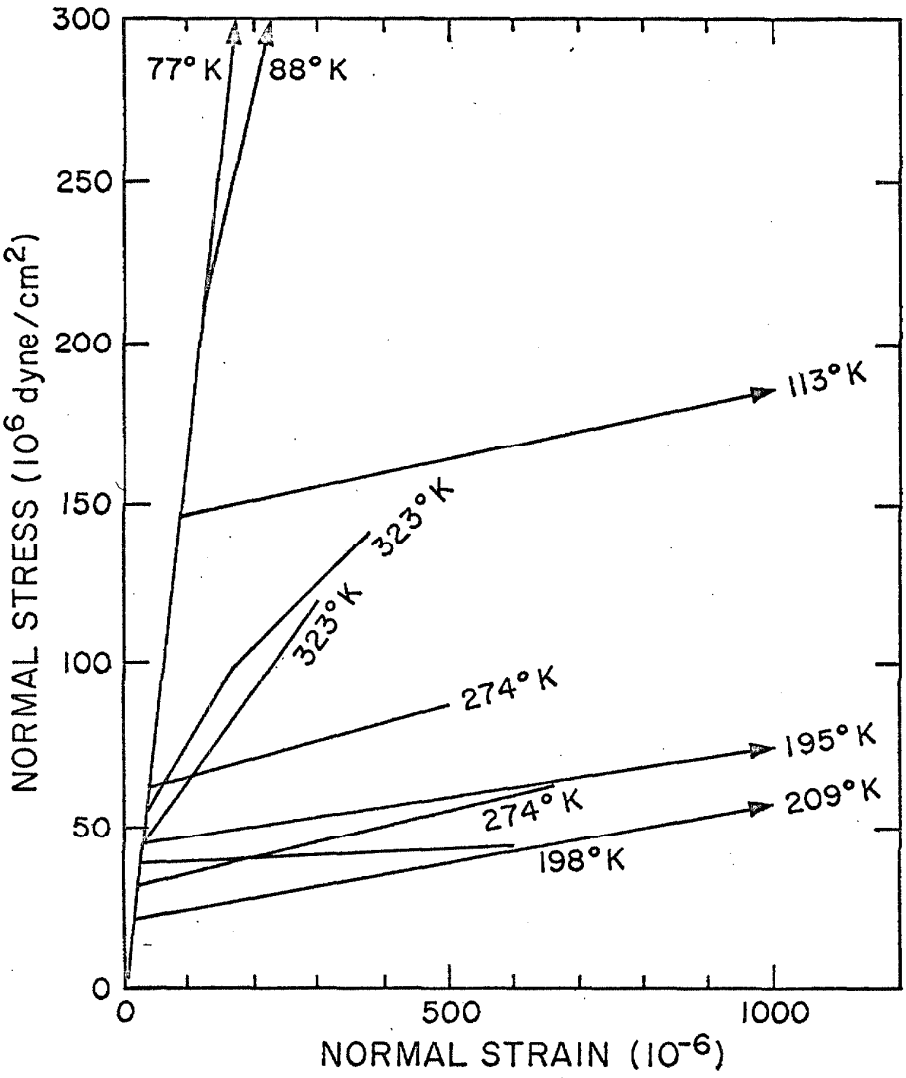

Figure 10 Stress-strain relations for various temperatures, arrows indicate that a larger stress or strain was attained

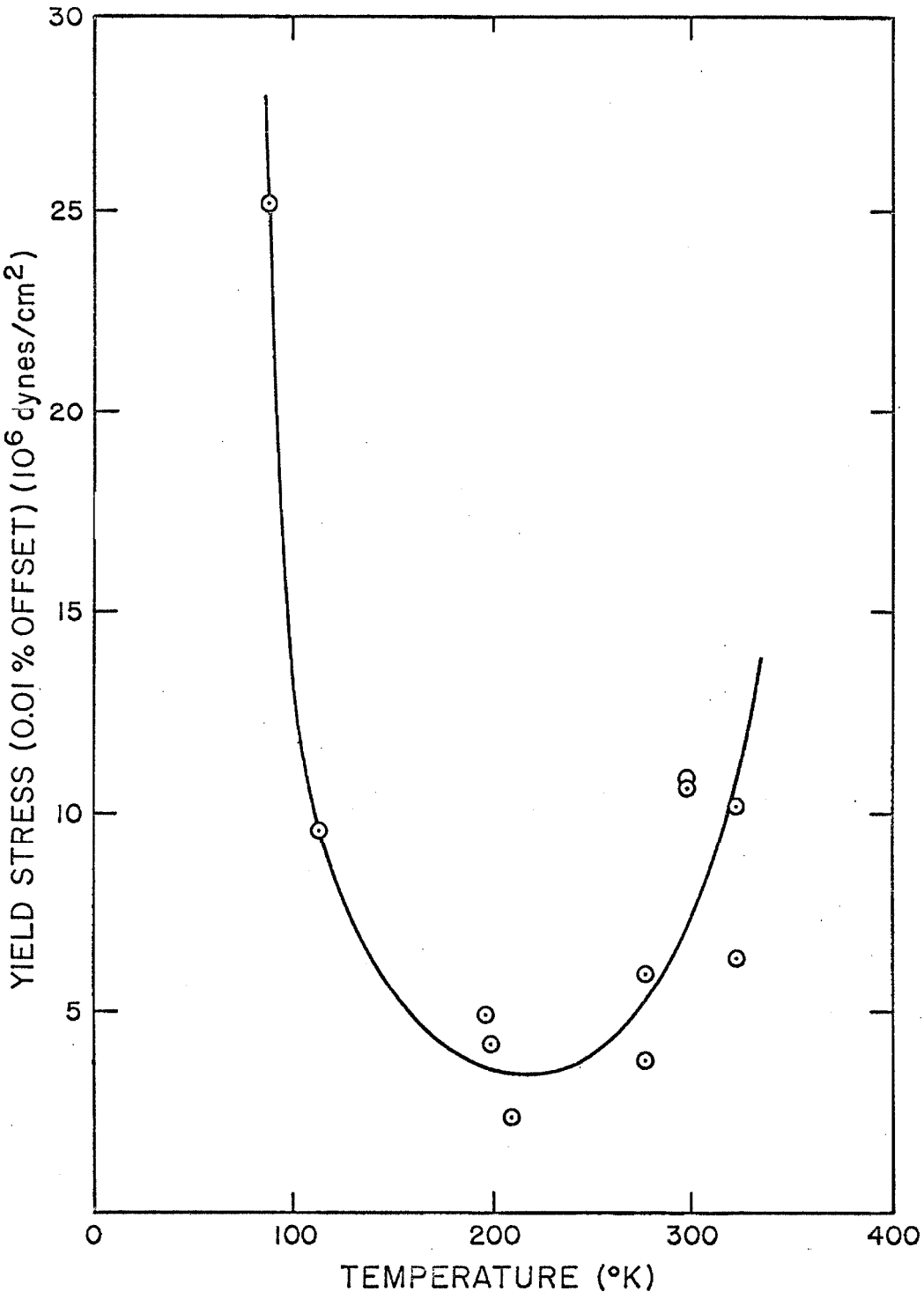

Figure 11 Stress to produce 0.01% plastic strain vs temperature

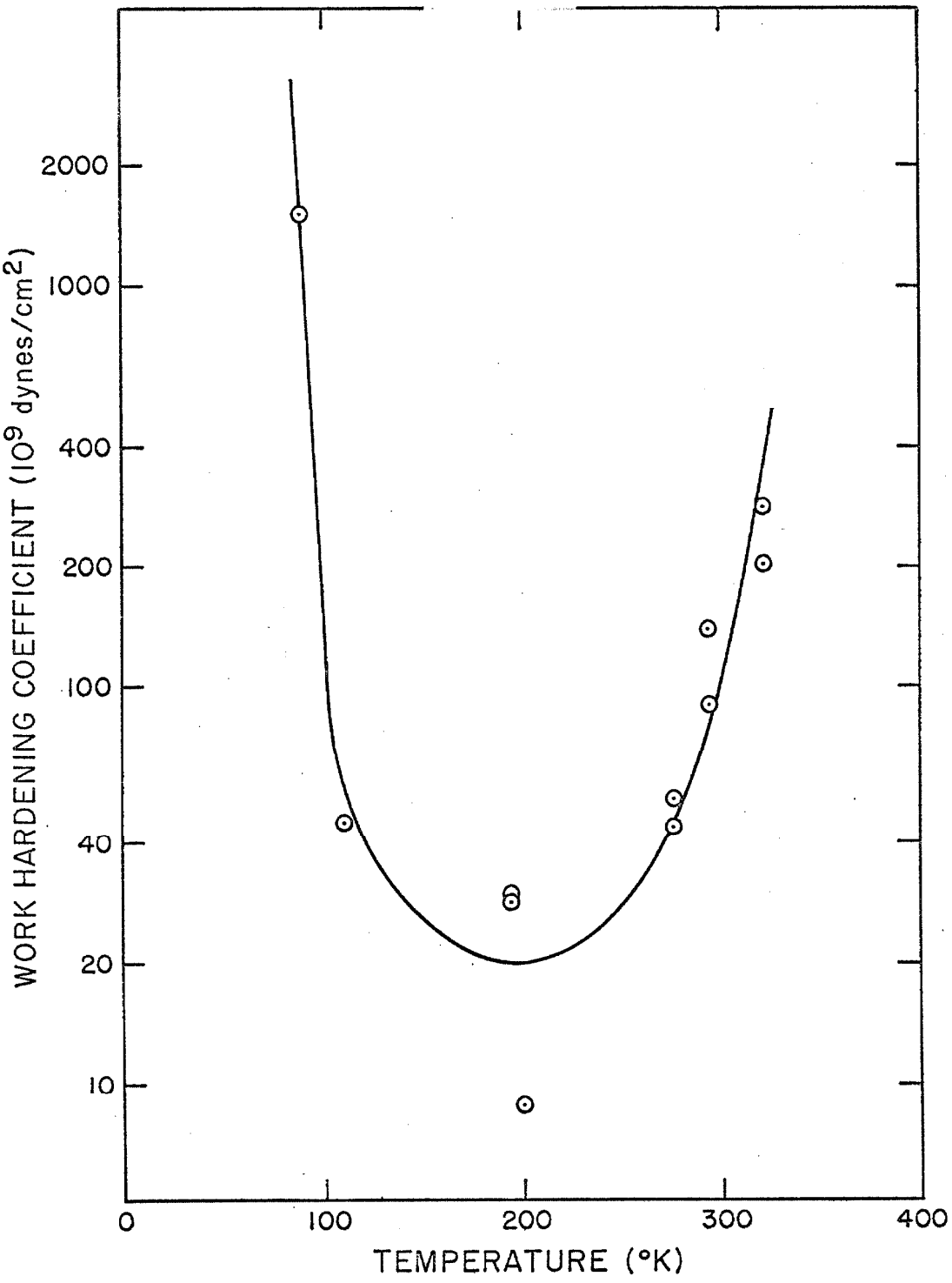

Figure 12 Work hardening coefficient as a function of temperature

V DISCUSSION

Validity of the Measured Dislocation Velocity

The validity of the assumption used in relating dislocation displacements to velocity will now be discussed. It was assumed that velocity is constant in time. This implies that the acceleration to a terminal velocity takes place in a small fraction of the pulse duration. This is a commonly used assumption and has been verified in several materials (17). In addition, no systematic variation in computed velocity was found with changes in stress pulse duration, so the assumption appears justified in the present case.

The observed scatter in the measurements of dislocation velocity vs stress, as shown in Figures 7, 8 and 9, will now be disucssed before we consider the possible mechanisms which might control the velocity of the dislocations. Figures 7, 8 and 9 show that the scatter was nearly the same for tests at different temperatures, that is, it was independent of the sensitivity of dislocation velocity to stress (mobility exponent), which varies greatly depending on the temperature. The mobility exponent is only one for temperatures of 110°K and below, whereas it reaches 23 for 323°K. Any stress concentration or bending would cause extreme variations in measured dislocation velocity for the case in which velocity depends on the 23rd power of stress. Since extreme variations of velocity were not observed, the simple compression stress state must have been closely approximated.

It is postulated that the variation of measured dislocation

velocities on any one test is caused by our inability to observe the maximum length of slip bands which are initiated by sources within the crystal. The maximum extent of the longest slip bands was taken to minimize this error. It is likely that the longest slip bands had sources which were located on the observation surface. Thus the true dislocation velocity is probably the maximum measured value at any given stress.

The variation in dislocation velocity from one test to another (about ± 15%) is attributed to slight differences in dislocation density and substructure in the high purity material employed in this investigation. Lavrent'yev and Salita (18) also found that the "starting stress" for pyramidal slip in zinc is structure-sensitive. The variation of their measurements on relatively low purity zinc was approximately a factor of two to three in stress. Adams (13) also made measurements very similar to those presented in this investigation and found approximately the same magnitude of variation from one test to another as that observed here. Furthermore, the stress level in Adams' tests was about a factor of two more than that reported here for the same dislocation velocity, again because of differences in structure. Adams employed spark erosion techniques for specimen preparation (see Turner (19) for documentation of the damage induced by spark machining), whereas acid lapping was employed in this investigation.

Comparision of Pyramidal and Other Kinds of Slip

Pyramidal slip has both similarities and differences compared

with other forms of slip. Pyramidal slip in zinc can be compared to that in the "hard" (not close-packed) materials with regard to the large yield stress and the small dislocation velocity near the yield stress in comparison with the "soft" (close-packed) materials. The yield stress for pyramidal slip in zinc ("hard") is about 10 to 20 times that for basal slip ("soft"). Figure 13 shows the (geometric) mean of edge and screw dislocation velocities for pyramidal slip near the room temperature yield stress. Dislocation velocity varies from 10^{-6} to 10^{-2} cm/sec, depending on temperature, whereas dislocation velocity near the yield stress for the "soft" materials is about 100 cm/sec (14,20). On page 44 of reference (14) Pope presents a table containing a more complete comparision of dislocation velocities in various materials.

The "hard" materials are generally characterized by large mobility exponents (sensitivity of dislocation velocity to stress) and large work hardening coefficients relative to the "soft" materials. Pyramidal slip also fits into the class of "hard" materials with regard to these characteristics.

However, pyramidal slip is unlike slip in either "hard" or "soft" materials with regard to the temperature dependence of dislocation velocity, yield stress, and the work hardening coefficient. In all other materials all of these quantities are monotonic functions of temperature. The velocity of pyramidal slip dislocations for a given stress increases with increasing temperature (normal), but then reaches a maximum and decreases with further increase of tem-

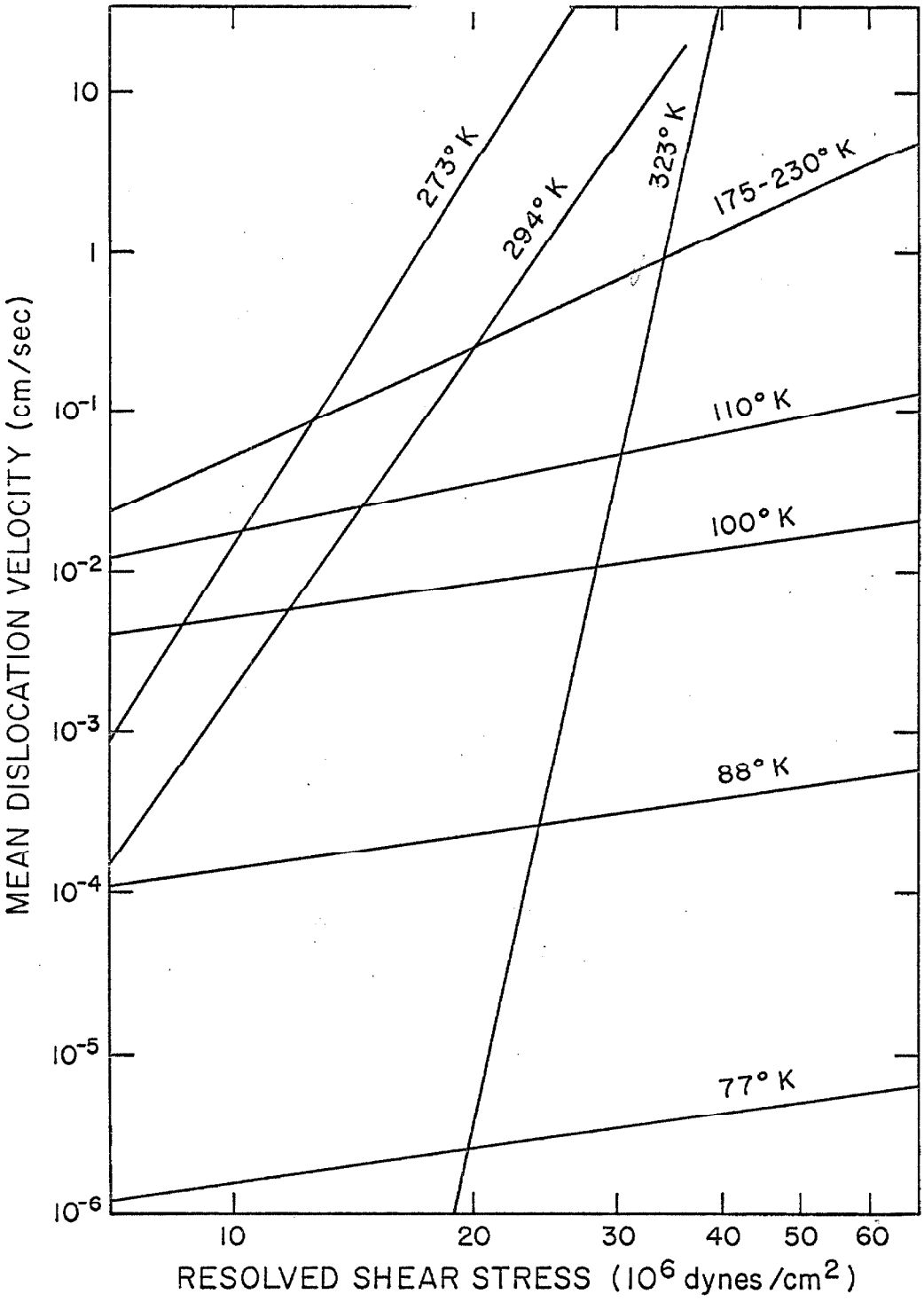

Figure 13 Mean dislocation velocity vs stress and temperature

perature (unique). This behavior is illustrated by the constant dislocation velocity contours which are shown in Figure 14 as a function of stress and temperature. It is also observed that "yield stress" and the work hardening coefficient exhibit the same sort of behavior as a function of temperature (see Figures 11, 12 and 14).

Dislocation Velocity for 77° to $110^{\circ}K$

It was found that dislocation velocity for the temperature range of 77° to $110^{\circ}K$ can be represented by an equation of the form $v = K\ \tau\ \exp(-U/kT)$ where v is dislocation velocity, K is a constant, τ is resolved shear stress, U is activation energy, k is Boltzmann's constant, and T is absolute temperature. Straight lines which represent equations of this form are shown in Figure 15 together with the experimental data. Numerical values for the activation energy are obtained from the slope of the curve of $\log_{10} v/\tau$ vs $1/T$, $U = -2.3K\ d(\log_{10} v/\tau)/d(1/T)$. It is found that $U_{screw} = 0.179$ ev and $U_{edge} = 0.184$ ev. The intercepts of the two curves on the ordinate axis give the values of K, the pre-exponential factor. It is observed that $K_{edge} = K_{screw} = 1\ (g/cm^2 sec)$.

Haasen (21) has observed the same functional form for dislocation velocity in germanium and has attributed the rate-limiting process to thermally activated formation of double kinks. Analysis of such a process involves consideration of the Peierls force, that is the lattice resistance to dislocation motion.

A Peierls mechanism is concerned with the probability that a

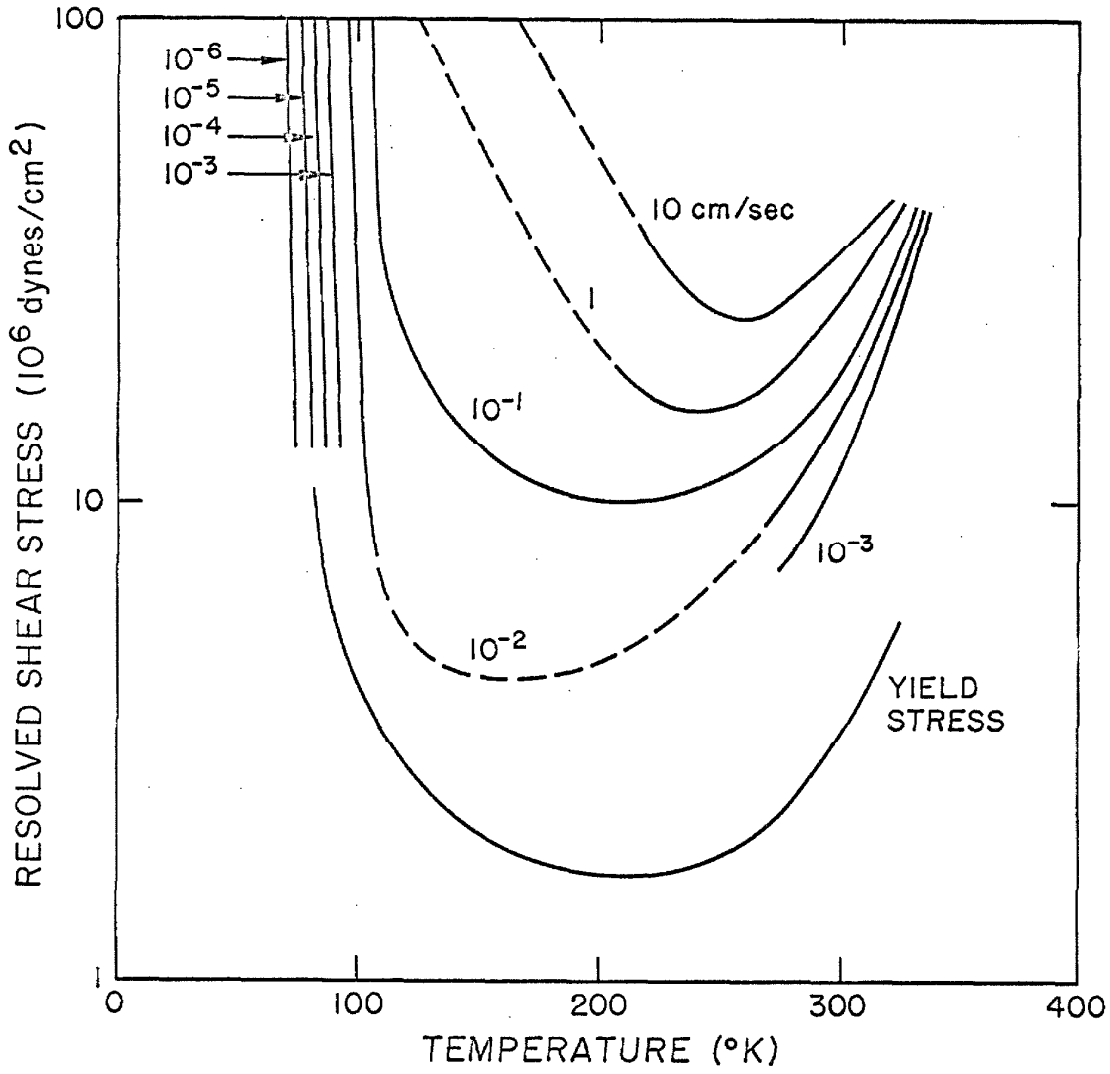

Figure 14 Constant dislocation velocity contours as a function of stress and temperature; the yield stress (resolved shear) contour is derived from Figure 11

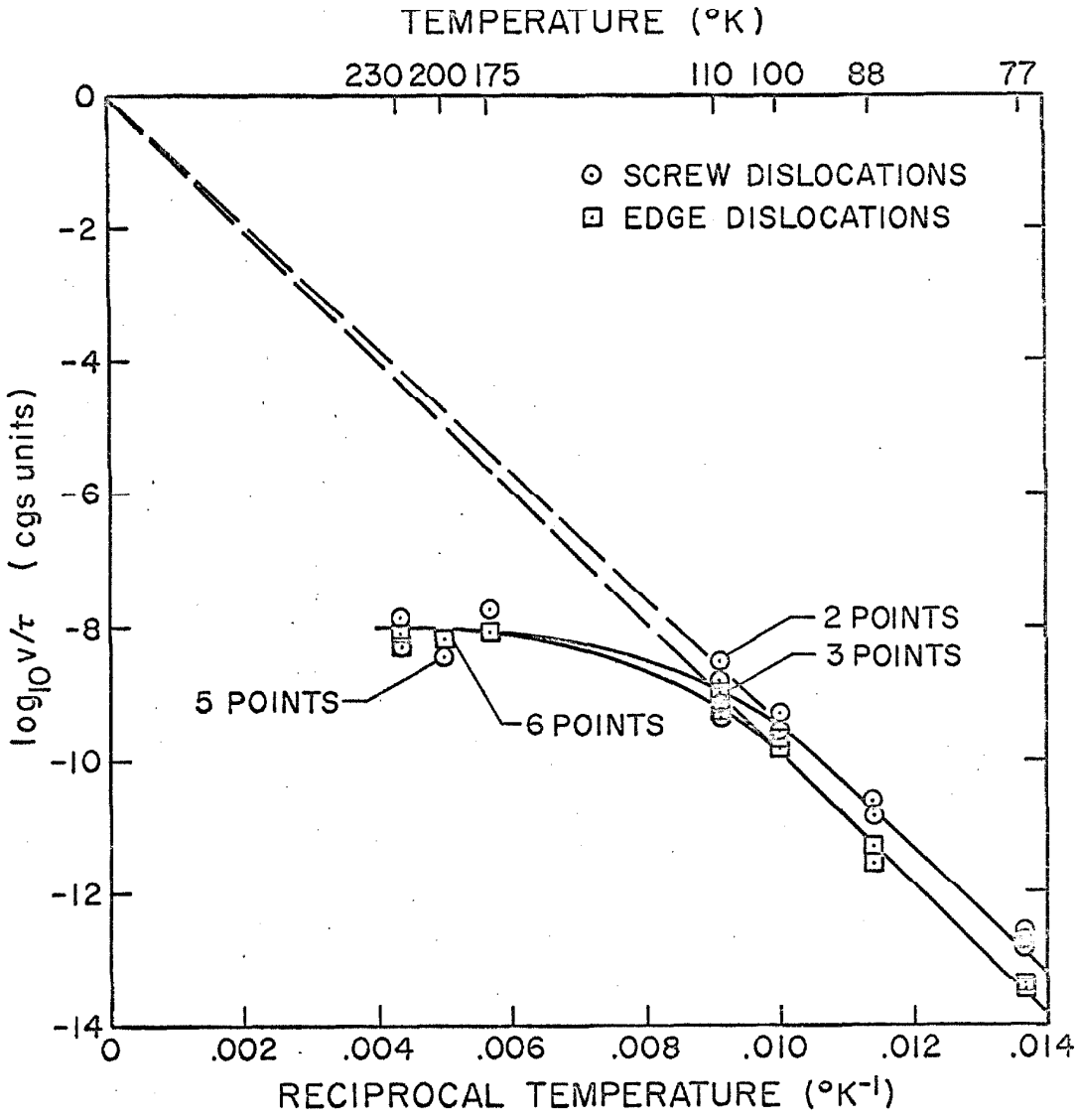

Figure 15 $(10\bar{1}\,24)$ surface, $\bar{a}$ vertical, slip bands formed on specimen 35-6 at 200°K, 31.0 Mdyne/cm^2, 0.346 sec, 50X

dislocation line may overcome the lattice potential and move foward one lattice parameter with the aid of thermal energy and the applied shear stress. Each treatment of the Peierls mechanism (see references (22, 23, 24) for examples of different approaches) considers the probability of nucleating a critical "double kink" in the dislocation line. A double kink on a dislocation line lying along a lattice potential minimum consists of two single kinks which link a short segment of dislocation line line lying along the next lattice potential minimum with the rest of the dislocation line. The critical double kink is defined as the one which will be able to grow without limit under the applied stress alone. After the two kinks have been driven apart by the applied stress, the dislocation line has advanced one lattive parameter in the direction of the applied stress.

The difficult nature of a quantitative formulation of this process can be appreciated when one considers the following factors. The probability of a successful movement of the dislocation line by one lattice parameter in the direction of the applied stress is the product of the attempt frequency and the probability that any given attempt will succeed. The attempt frequency depends on the critical kink size and the lattice vibration frequency. The probability of success depends on the activation energy for the double kink configuration as modified by the applied stress. The net velocity may also depend on the probability that a double kink may be nucleated in the direction opposing the stress. All of these factors are interdependent and elasticity theory cannot be

applied to the problem because the strains are too large. The net result of all the considerations is that no Peierls formulation is yet available, which can predict the quantitative features (or the functional form) of the data presented above.

Although a quantitative fit to a Peierls mechanism cannot be accomplished at this time, other indications imply that this is the proper mechanism. For example, it is found that the activation energy, U, is independent of stress and temperature, hence it must be related to a lattice potential. It will also be shown that the critical double kink size is very small, which implies that the mechanism is characterized by a process which takes place on such a small scale that the impurity, obstacle, or intersection mechanisms can probably be ruled out. The classical formula for Peierls limited dislocation velocity is $v/v_o = \exp(-1/kT)(U - \tau bA)$ where τbA is the work done by the applied stress as the critical double kink forms, and A is the area of the double kink. Differentiation of $\ln(v/v_o)$ with respect to τ allows us to obtain the following,

$$\frac{\partial \ln v/v_o}{\partial \tau} = \frac{Ab}{kT}$$

$A = 2b^2$ upon substitution of numerical values from the data. Hence, the critical spacing of the kinks is about 2b. This kink spacing is much too close to allow use of elasticity theory. This is the root of the problem for the quantitative treatment of the Peierls

barrier.

A possible explanation for the larger screw dislocation velocity is now advanced. Price (10) observed edge-type pyramidal slip dislocations dissociate on the basal plane. This implies that the stacking fault energy is lower for an edge dislocation (on the basal plane) than for a screw dislocation. Hence, edge dislocations should be extended more than screw dislocations and it should then require more energy to constrict the fault ribbon of a dissociated edge dislocation than for a screw dislocation. The larger constriction energy for the edge dislocation influences the activation energy in a Peierls formulation because the dislocation must first be constricted (to become glissile) before the double kink can be nucleated. In other words, additional energy must be supplied to nucleate a double kink on an edge dislocation and it would be expected that the activation energy for edge dislocation movement should be larger than for screw dislocations.

Examination of the data indicates that a difference in activation energy (different slope of $\log_{10} v/\tau$ vs $1/T$) for edge and screw dislocations is sufficient to account for the observed difference between edge and screw dislocation velocity. It is, in fact, observed that U_{edge} is greater than U_{screw} and the difference in dislocation velocity is not caused by different pre-exponential factors K_{edge} and K_{screw}. It should be mentioned that the straight lines in Figure 15 were drawn to show that different activation energies could provide a possible explanation for the difference of edge

and screw dislocation velocities. Although the difference in activation energies is small, it appears to be significant.

Dislocation Velocity Above 110°K

The deviation from linearity in Figure 15 shows that there is a source of drag in addition to that of the Peierls barrier at temperatures above 110°K. It is also observed that slip bands become continually wider above this temperature. This indicates the presence of an increasing amount of cross-glide which may be aided by thermal activation, hence an increase in temperature would cause more cross-glide. Double cross gliding screw dislocations leave behind the dipole trails observed by Price (10). The number of these dragging dipole trails increases with increasing temperature (more cross-glide), so the screw dislocations are retarded.

Edge dislocations do not cross-glide so they are not subject to drag from the trailing dipoles directly, however, the edge dislocations (those dislocations observed on the $(10\bar{1}0)$ surface) are observed to slow down with increasing temperature also. It is argued that dislocations are not greatly constrained to lie in a Peierls valley at temperatures as high as 0.3 to 0.5 to T_{melt}, which is the range in which velocity decreases as temperature increases. Hence, the dislocations in the slip band have a wavy shape everywhere and dislocation velocity is dictated by the slowest (screw) velocity.

Dislocation Dynamics and Macroscopic Tests

The observation of dislocation velocity as a function of stress

and temperature can be used to understand some peculiar features of the stress vs strain relations. For example the "yield stress" shows a sharp minimum with respect to temperature (see Figure 11). This is explained by considering dislocation velocity as a function of temperature for a given low stress such as 10 Mdyne/cm^2. It will be noticed that velocity vs temperature has a maximum at approximately the same temperature that the yield stress shows a minimum. These extrema are consistent because a larger dislocation velocity permits a larger plastic strain rate earlier in the stress-strain test (see Johnston (17)). This will be manifested by a smaller "yield stress". Similarly, the exceedingly small dislocation velocity at 77°K (very low plastic strain rate) explains why no plastic strain was detected on these tests, even on a crystal which had been deliberately strained at a higher temperature to increase the dislocation density. Similarly, dislocation velocity becomes very small at low stresses for room temperature and above, and again the "yield stress" increases for the same reason that it did at low temperature.

A quantitative evaluation of the "yield stress" is complex because of the influence of the testing machine together with the crystal and also because of the unknown number of mobile dislocations. For example, the coutour labeled "yield stress" in Figure 14 (0.01% plastic strain) is now a resolved shear stress on the pyramidal slip planes and is derived from Figure 11. This shows that measurement of a "yield stress" may not be quantitatively equivalent to any

particular dislocation velocity. Lavrent'yev, et al. (25) measured a "starting stress" for pyramidal slip in pure bending as a function of temperature. Their results grossly overestimate the "starting stress" at low temperatures, because they did not allow sufficient time for the dislocations to move to their equilibrium positions relative to the neutral axis of the beam. They took the stress in the beam at the observed positions as equal to the "starting stress" and found it to be 130 Mdyne/cm^2 at 77^{o}K, whereas in this investigation dislocation movement was detected at 77^o K for a stress of only 16 Mdyne/cm^2.

The work hardening coefficient vs temperature (Figure 12) shows the same type of behavior as the "yield stress". The work hardening coefficient also has an apparent high value at low temperatures because dislocation velocity is so small that the equilibrium strain was not attained at any given stress. Hence, the true work hardening coefficient is not measured in a low temperature test because the equilibrium ("static") test was not achieved. As the temperature is increased a better approximation to the "static" stress-strain curve is obtained because dislocation velocities permit a closer approach to equilibrium. However, the real increase in the work hardening coefficient with temperatures above 200^{o}K must be explained by the debris left behind as dipoles quickly transform into stacking fault loops on the basal plane (10). A further increase in temperature should eventually cause a decrease in the work hardening coefficient because of the advent of creep processes. Gilman (8)

observed this decrease in the work hardening coefficient at about 373°K (about 0.54 T_m).

Effect of the Stress State

Gilman (8) found different behavior for $\bar{a}$ axis tension and compression stress-strain curves, however, Stofel and Wood (7) found no difference between $\bar{c}$ axis tension and compression stress-strain curves. Lavrent'yev and Salita (18) measured a "starting stress" for pyramidal slip in pure bending tests and observed dislocation motion on both the tension and compression sides of a beam specimen. In addition, no difference in dislocation velocity for $\bar{c}$ axis compression, $\bar{a}$ axis tension, or $\bar{a}$ axis compression was found in this investigation. Therefore there is good reason to doubt Gilman's observation of a different material behavior depending on the sense of stress.

VI SUMMARY AND CONCLUSIONS

The velocity of pyramidal slip dislocation in slip bands in single crystals of 99.999% pure zinc was measured as a function of stress and temperature. For temperatures of 77° to 110°K the resistance to the motion of edge and screw dislocations was attributed to a Peierls mechanism for which the activation energy was 0.182 ev. For this temperature range it was found that dislocation velocity was directly proportional to the stress and that screw dislocations moved more rapidly than edge dislocations for a given stress and temperature. The dislocation velocity was found to increase less rapidly with increasing temperature above 110°K. In fact, the dislocation velocity reached a maximum with increasing temperature, for a given stress, and then decreased with further increase of temperature. It was also found that the slip bands become increasingly wide above 110°K. Hence it is postulated that the amount of cross glide increases with temperature. Price (10) has shown that cross-gliding pyramidal slip dislocations leave behind dragging dipole trails. Therefore, it is postulated that the dragging dipole trails account for the decrease in velocity with increasing temperature above 110°K.

Experimentally measured dislocation velocities are used to account for the anomalous temperature dependence of macroscopic stress-strain relations for zinc deformed by pyramidal slip.

Suggested Further Work

More experimental work would be very desirable, particularly

with regard to additional measurements of dislocation velocity at temperatures of 110°K and less, to determine the stress dependence more accurately. Transmission electron microscopy should be employed to give experimental data on the free lengths and orientation of pyramidal slip dislocations. This data would greatly facilitate the formulation of a model which would predict the experimental observations. Transmission electron microscopy and theoretical would could equally well be applied to a quantitative formulation for the progressive retardation of the dislocations as the temperature is increased.

APPENDIX A

X-ray Diffraction Microscopy and Etch Pitting to Reveal Dislocations

The Berg-Barrett (B-B) technique (14) was used because it is difficult to reveal dislocations by etching the $\{10\bar{1}\,24\}$ surfaces (13). Hence, B-B was sometimes used to supplement the information which could be gained by etching these planes. After the etching technique was improved the B-B micrographs were abandoned because of the long exposure (7 hours) required.

The B-B micrographs were valuable for two purposes; they gave information that could not always be obtained by etching, and a comparison of the micrograph and the etched surface shows that the etch pitting does reveal dislocations. However, general pitting of the $\{10\bar{1}\,24\}$ surface occurs when the crystal is polished longer than about 2 sec, and this pitting does not correspond to dislocations intersecting the surface. Figure A-1 shows the correspondence between a B-B micrograph and the etch figures produced after the micrograph was made.

The diffraction conditions used to obtain the x-ray micrograph are described by Pope (14). However, Pope was interested in observing basal dislocations which lie parallel to his basal observation surface. Screw oriented pyramidal slip dislocations intersect the $\{10\bar{1}\,24\}$ surface at a large angle (60°). Nevertheless, the pyramidal slip dislocations (in slip bands) could be seen as very closely spaced spots in spite of the small depth of penetration (5 - 10 μ) for

a

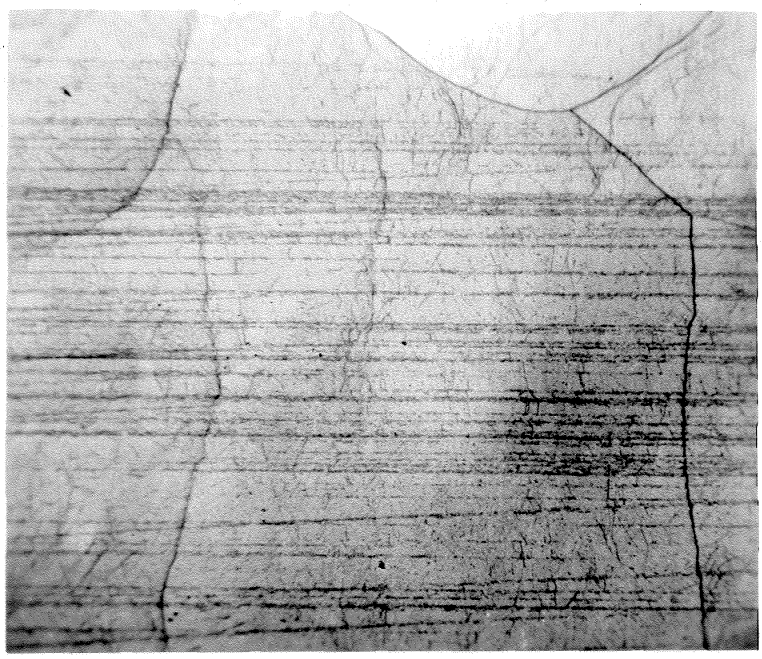

b

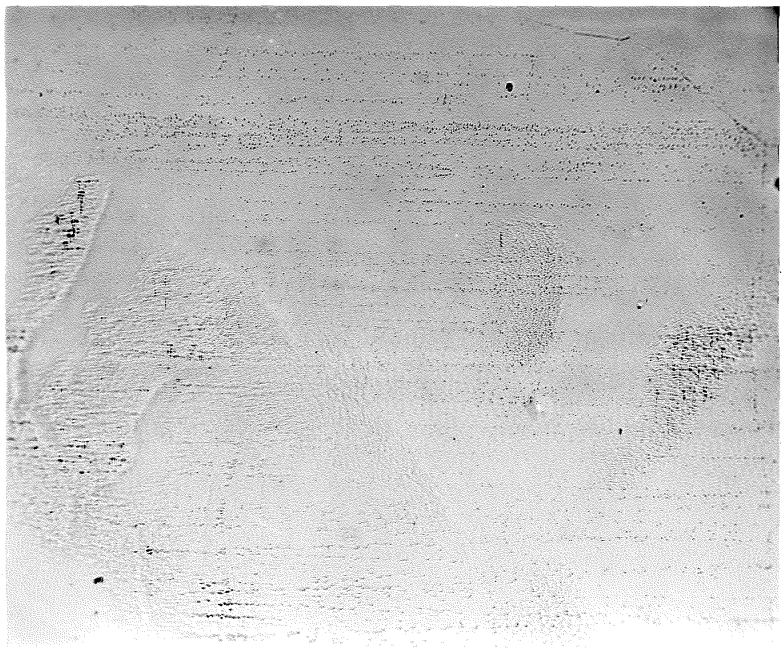

Figure A-1 $(10\bar{1}\,24)$ surface, $\bar{a}$ vertical, slip bands formed on specimen 35-6 at 200°K, 31.0 Mdyne/cm^2, 0.346 sec , 50X
a) X-ray micrograph b) Etch pitted

the x rays. Basal dislocations can be seen in Figure A-1a (a $\{10\bar{1}3\}$ reflection) as vertical segments. (These dislocations did not give a contrast effect when (0002) diffracting planes were employed, so these dislocations must have a Burgers vector which lies in the basal plane.)

APPENDIX B

Observation and Discussion of Twinning

Crystals oriented for $\bar{c}$ axis compression tests at room temperature consistently twinned upon application of stress pulses of an amplitude of 50 Mdyne/cm^2 or greater. This behavior was unexpected because twinning was not observed at stresses below 150 Mdyne/cm^2 in similar pulse tests performed by Adams (15). Bell and Cahn (9) also found that a much larger stress was necessary to initiate the first twins in a zinc crystal.

The twinning behavior of the crystals was observed to have a strong dependence on loading rate. The crystals could be subjected to a stress as large as 120 Mdyne/cm^2 in a slow loading test using a crosshead speed of 0.0025 cm/min in an Instron, whereas a crosshead speed of 0.010 cm/min caused twinning at only 50 Mdyne/cm^2. The pulse tests mentioned above correspond to a very fast loading rate.

The effect of loading rate on the twinning behavior may be explained by a relaxation of possible stress concentrations (where twins might be nucleated) which could be accomodated by pyramidal slip in the slower, but not in the faster tests. However, relaxation does not explain the larger twinning stress for Adams' spark machined crystals, for which dislocation density was higher and pyramidal slip dislocations moved more slowly compared with the crystals employed in this investigation. Therefore, there must be a real effect upon twinning behavior resulting from the different initial dislocation structures.

LIST OF REFERENCES

1. W. G. Johnston and J. J. Gilman, "Dislocation Velocities, Dislocation Densities, and Plastic Flow in Lithium Fluoride Crystals," J. Appl. Phys. 30, 129 (1959).

2. J. C. M. Li, "A Dislocation Mechanism of Transient Creep," Acta Met. 11, 1269 (1963).

3. J. W. Taylor, "Dislocation Dynamics and Dynamic Yielding," J. Appl. Phys. 36, 3146 (1965).

4. F. R. N. Nabarro, Z. S. Basinski, and D. B. Holt, "Plasticity of Pure Single Crystals," Advan. Phys. (Phil. Mag. Supplement) 13, 193 (1964).

5. A. Seeger, "Work Hardening of Metal Single Crystals, Slip Lines, and Transmission Electron Microscopy," The Relation between the Structure and Mechanical Properties of Metals, London: Her Majesty's Stationery Office, 4 (1963).

6. U. F. Kocks, "Statistical Treatment of Penetrable Obstacles," Can. J. Phys. 45, 737 (1967).

7. E. J. Stofel and D. S. Wood, "Fracture of Zinc Single Crystals," Fracture of Solids, publ. Interscience, 521 (1963).

8. J. J. Gilman, "Study of a New Mode of Plastic Deformation in Zinc Crystals," Trans. AIME, J. Metals 203, 206 (1955).

9. R. L. Bell and R. W. Cahn, "The Dynamics of Twinning and the Interrelation of Slip and Twinning in Zinc Crystals," Proc. Roy. Soc. (London) A239, 494 (1957).

10. P. B. Price, "Pyramidal Glide and the Formation and Climb of Dislocation Loops in Nearly Perfect Zinc Crystals," Phil. Mag. 6, 873 (1961).

11. J. J. Gilman, "Plastic Anisotropy of Zinc Monocrystals," Trans. AIME, J. Metals 206, 1326 (1956).

12. R. C. Brandt, K. H. Adams, and T. Vreeland, Jr., "Dislocations and Etch Figures in High Purity Zinc," J. Appl. Phys. 34, 591 (1963).

13. K. H. Adams, R. C. Blish, II, and T. Vreeland, Jr., "Orientation Dependence of a Dislocation Etch for Zinc," J. Appl. Phys. 37, 4291 (1966).

14. D. P. Pope, "Mobility of Edge Dislocations in the Basal Slip System of Zinc," Ph.D. Thesis, California Institute of Technology, Pasadena, California (1967).

15. K. H. Adams, "Dislocation Mobility and Density in Zinc Single Crystals," Ph.D. Thesis, California Institute of Technology, Pasadena, California (1965).

16. T. L. Russell, D. S. Wood, and D. S. Clark, "The Influence of Grain Size on the Yield Phenomenon in Steel," Acta Met. 9, 1054 (1961).

17. W. G. Johnston, "Yield Points and Delay Times in Single Crystals," J. Appl. Phys. 30, 129 (1959).

18. F. F. Lavrent'yev and O. P. Salita, "Pyramidal Slip in Zinc Crystals," Soviet Phys. - Cryst. (USA) 8, 803 (1964).

19. A. P. L. Turner, K. H. Adams, and T. Vreeland, Jr., "Damage Due to Electric Spark Discharge Machining of Zinc," Materials Science and Engineering 1, 70 (1966).

20. W. F. Greenman, "Dislocation Mobility in Pure Copper Single Crystals," Ph.D. Thesis, California Institute of Technology, Pasadena, California (1966).

21. P. Haasen, "Dislocation Dynamics in the Diamond Structure," Battelle Colloquium on Dislocation Dynamics, May 1967, to be published by McGraw-Hill (1968).

22. J. E. Dorn and S. Rajnak, "Nucleation of Kink Pairs and the Peierls' Mechanism of Plastic Deformation," Trans. AIME 230, 1052 (1964).

23. A. Seeger and P. Schiller, "Bildung und Diffusion von Kinken als Grundprogress der Versetzungbewegung bei der Messung der Inneren Reibung," Acta Met. 10, 348 (1962).

24. J. Friedel, "On the Elastic Limit of Crystals," in Electron Microscopy and Strength of Crystals, ed G. Thomas and J. Washburn, Interscience publ., 605 (1963).

25. F. F. Lavrent'yev, O. P. Salita, and V. I. Startsev, "Dependence of the Starting Stress for Pyramidal Dislocations on the Temperature and Degree of Perfection of Zinc Crystals," Soviet Phys. - Cryst. (USA) 10, 95 (1966).